

## Parametric Structural Optimization of 2D Complex Shape Based on Isogeometric Analysis

Long Chen<sup>1</sup>, Li Xu<sup>1</sup>, Kai Wang<sup>1</sup>, Baotong Li<sup>2,\*</sup> and Jun Hong<sup>2</sup>

<sup>1</sup>School of Mechanical Engineering, University of Shanghai for Science and Technology, Shanghai, 200093, China

<sup>2</sup>Key Laboratory of Education Ministry for Modern Design & Rotor-Bearing System, Xi'an Jiaotong University, Xi'an, 710049, China

\*Corresponding Author: Baotong Li. Email: baotong.me@mail.xjtu.edu.cn

Received: 25 January 2020; Accepted: 23 March 2020

**Abstract:** The geometric model and the analysis model can be unified together through the isogeometric analysis method, which has potential to achieve seamless integration of CAD and CAE. Parametric design is a mainstream and successful method in CAD field. This method is not continued in simulation and optimization stage because of the model conversion in conventional optimization method based on the finite element analysis. So integration of the parametric modeling and the structural optimization by using isogeometric analysis is a natural and interesting issue. This paper proposed a method to realize a structural optimization of parametric complex shapes by using isogeometric analysis. By the given feature curves and the constraints, a feature frame model is built. Based on the feature frame model, a parametric representation of complex shape is obtained. After adding some auxiliary curves, the feature frame model is divided into many box-like patches in three dimension or four-sided patches in two dimension. These patches are built into parametric patches by using volume interpolation methods such as Coons method. Based on the parametric patches, isogeometric analysis is applied. Thus, the relationships are constructed among the size parameters, the control points and the physical performance parameters. Then the sensitivity matrix could be derived based on the relationships. The size optimization is carried out in the first stage by taking the size parameters as variables. Based on the result of size optimization, shape optimization with the constraints of stress is carried out in the second stage by taking the control points as variables. Several planar complex shapes are taken as example to verify our method. The results verify that the parametric modeling and structural optimization can be united together without model conversion. Benefit from this, the optimization design can be executed as a dark box operation without considering the concrete modeling and analysis by input of the sizes, constraints and loads.

**Keywords:** Isogeometric analysis; parametric design; structural optimization; sensitivity analysis; complex shape



This work is licensed under a Creative Commons Attribution 4.0 International License, which permits unrestricted use, distribution, and reproduction in any medium, provided the original work is properly cited.

## 1 Introduction

In the stage of product optimization design, phase, the initial CAD model can be optimized based on the results obtained during the simulation analysis phase. The optimal CAD model improves the performance of the CAD products [1–4]. Structural optimization has always been an important research area because it usually attempts to integrate structural analysis, optimization algorithms and geometric modeling into an automated design. The main purpose of structural optimization is to improve structural characteristics, such as reducing the stress concentration and weight, and increasing the stiffness by changing the structure boundary geometry. Optimization is divided into three stages: size optimization, shape optimization and topology optimization [5]. Topological optimization is to determine the best product prototype by changing the topological structure according to the best force transmission path in a given material design domain. Shape optimization takes the boundary shape of the structure as the optimization object. It takes the node coordinates as the design variables. Finally it improve the performance of product by changing the boundary shape [6–7]. Size optimization is the optimization of discrete dimensional variables to determine the final accurate dimensional model of the product.

In traditional structural optimization, the design model is converted into the finite element model in the process of applying FEA method. Transformation of design model, analysis model and optimization model leads to inaccuracy and tediousness. In order to describe the boundaries to be optimized, earlier method took node coordinates as design variables [8]. Taking the node coordinates of finite element model has the following disadvantages [11]. Firstly, a large number of design variables are needed to describe the shape of the boundary. Secondly, the independent changes of each node in the optimization iteration can easily lead to grid distortion and distortion. Thirdly, the model of design, analysis and optimization are not unified, so that data transmission can only be unidirectional.

Isogeometric optimization method has received more and more attentions recently [9–10]. Benefiting from the superiority of splines in shape expression, shape optimization based on isogeometric Analysis has achieved great success [12–13]. However, the current isogeometric analysis and optimization methods encounter difficulties when facing the complex shapes or models because of the complexity existing in the stage of construction and analysis.

For the 2D complex shapes, we do not directly treat design model but its feature frame model as the optimization object. In this way, the design variables are greatly reduced. The optimization object is closer to the designer's intent since the feature sizes of the product are mainly mainly the designer's concern. The feature frame model is used to control the shape of overall model and detail. The designer is allowed to edit the product model by a few feature parameters. Thus, the parametric modeling based on feature sizes and the optimization based on the parametric model are unified together. The contributions of this paper as follows:

1) A framework supporting parametric modeling, isogeometric analysis and optimization is proposed. The framework supports to construct the relations existing among the design size variables, control points and physical performance parameters, which will help to derive the sensitivity matrix for optimization.

2) Structural optimization including shape and size optimization is realized with the help of sensitivity matrix to reach the optimization of global and local performance by taking the sizes and control points as the design variables.

## 2 Related Works

The isogeometric analysis method based on volume parametric model was first proposed by Hughes in 2005 [14]. Compared with other methods, he application of isogeometric analysis to product design has more advantages. The consistency of the design model and the analysis model are ensured, and the seamless integration between the models is achieved. It will obtain more precise result than the traditional finite

element method which uses geometry approximation. The current research topics of isogeometric analysis include: 1) the basic theory of isogeometric analysis, including accuracy calculation, convergence, continuity and singularity, and so on [15–16]; 2) improvement of Isogeometric analysis method, such as boundary element method, collocation method, etc. [17–18]; 3) extension of isogeometric analysis based on various spline basis functions [19–20]; 4) application of geometric analysis for various practical applications [21–22]. Before widely exploited in engineering field, isogeometric analysis of complex shapes is an important and necessary issue. Due to the inherent attribute of volume parameterization presented with tensor product, parameterization and analysis of complex shapes is a bottleneck problem. There have been some works that try to solve this problem, such as wear coupling and trimmed multi-patch merging or tearing [35–36].

We call the optimization method based on isogeometric analysis as isogeometric optimization, which has been carried out in the field of size optimization, shape optimization and topology optimization. Great research progress has been made in shape optimization based on isogeometric optimization benefiting from the superiority of splines in expressing shape [23–28]. There have some tentative studies on topology optimization, but the current research has not made much progress due to the limitations of the spline function in expressing topology [29–32]. There has few studies on size optimization based on isogeometric optimization [33,42–46], because it is not an intuitive way to present the curved shapes expressed as splines into sizes which are mostly horizontal, vertical, and angular. At the same time, the shapes expressed by splines are mostly free shapes, and parametric modeling of these shapes is not a trivial work. Since isogeometric optimization uses NURBS splines as basis function, which improves the continuity of the computational domain, sensitivity analysis becomes an important issue in isogeometric optimization problems [34].

### 3 Overview of Our Algorithm

In our method, a feature frame model composed of feature curves is firstly constructed. The feature curves can be acquired through given sizes or extracting from a point cloud model. A parametric feature frame model can be driven to modify by adding some constraints. Then the feature frame model is divided into many box-like subdomains by adding some curves. Volume interpolation such as Coons method and the optimization methods applied on the inner control points are used to create volumetric solid. By using the IGA method, displacement, stress and other physical parameters of each control point can be obtained after applying boundary conditions and constraints on to the analysis model [37]. The relationships between physical parameters and characteristic parameters are established. According to the above established relationships, the sensitivity matrix can be obtained by the derivatives of physical parameters with respect to feature parameters. Through the optimization algorithm and the sensitivity matrix, the feature parameters and the corresponding feature frame model are updated until the given iteration termination conditions are satisfied. The work process of product optimization design is shown in Fig. 1.

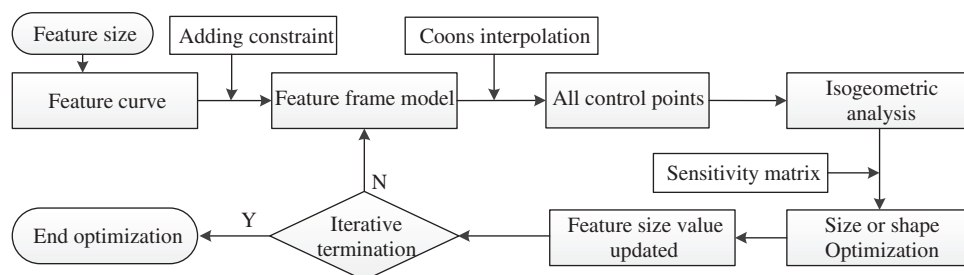


**Figure 1:** Flow chart of optimization process based on feature frame

## 4 Generation of 2D Parametric Complex Model

### 4.1 Domain Composition

The first step of the isogeometric analysis is creating the parametric computational domain. Computational domain with complex boundary or topology is supposed to be divided into multi parametric quadrilateral computational domains. This problem is similar to the domain decomposition method by dividing the solving region into a number of sub-systems or sub-regions according to some certain rules. The methods can be divided into two categories, non-overlapping subdomain decomposition and overlapping domain decomposition, as shown in Fig. 2. In the figure, (a) denotes the None-overlapping domain decomposition, (b) denotes the overlapping domain decomposition.

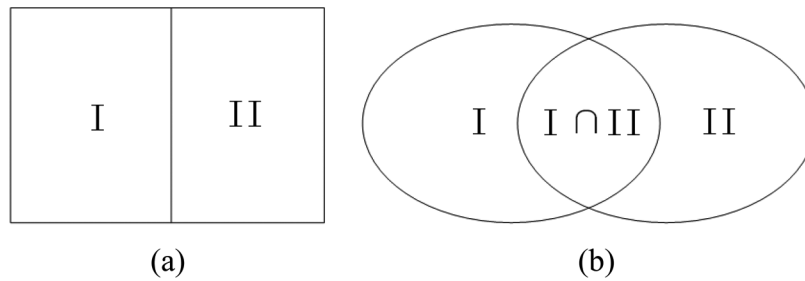


**Figure 2:** Decomposition with overlapping domains and non-overlapping domains

Assuming the computational domain  $\Omega$  is divided into a series of subdomain  $\{\Omega_i\}$ , the overall domain with overlapping domains can be expressed as follows:

$$\Omega = \Omega_1 \cup \Omega_2 \dots \Omega_n, \Omega_i \cap \Omega_j \neq \emptyset, i \neq j.$$

And the non-overlapping domain is,

$$\Omega = \Omega_1 \cup \Omega_2 \dots \Omega_n, \Omega_i \cap \Omega_j = \emptyset, i \neq j.$$

### 4.2 Parametric Modeling Method

In this paper, all the subdomains denote NURBS surfaces, so the objective of modeling is to construct these subdomains. A feature frame model is consisted of feature points, feature curves or feature surfaces. The feature points mainly emphasize the morphological location of details but they are inadequate to describe the whole shape. The shape of the surface has a specific function, which is synthesized by the feature curves. Though the whole content of the shape can be expressed, it is too over complicated and not easy to be operated. The feature curves contain important modeling information that can be linked to the feature points and the feature surfaces. They have no cumbersome operations caused by excessive number of points. They also have no redundancy of surfaces, so the processing of the feature curves is more superior to that of the feature points and feature surfaces.

Here, feature frame model is only composed of feature curves. The feature curves can be generated by curve parameterization method by giving the sizes. The feature curves can also be extracted from point cloud models. All the feature curves are linked by all kinds of geometric constraints. The whole process is depicted in Fig. 3.

When constructing the feature curve frame, the following basic principles should be considered when designing the characteristic curve: 1) Feature curves have semantic meaning in order to reflect the shape, size and position of the design object; 2) The feature curves are easy to edit in order to control the shape or size during the interactive operation; 3) The feature curves are simple in order to reduce the difficulty of modeling.

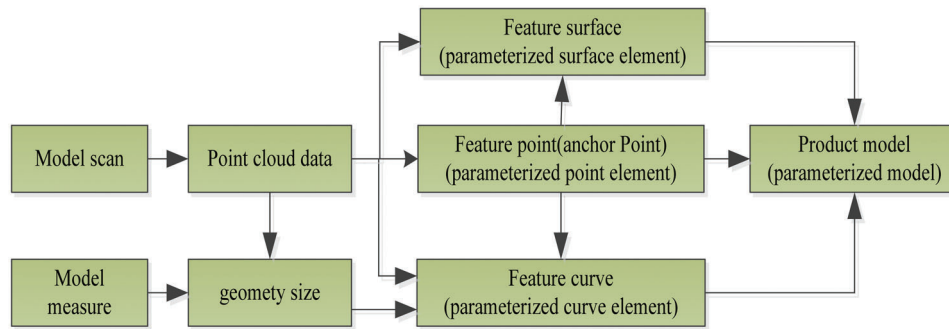


**Figure 3:** Construction of parametric model through feature elements

Following the three principles, the curves of profiles and sections are selected as feature curves, as well as the curves with design significance. The feature curves are stratified into geometric layer, constraint layer and semantic layer. The geometric layer is generally composed of control points, knot vectors or interpolation points. The layer constitutes the lowest level of the feature curve. The constraint layer is composed of the constraints of geometry, dimension and topology, which are generated during the process of generation and modification of feature curves. The semantic layer describes the semantic parameters and functions of the feature curves. The semantic parameters are defined for the control feature curves according to the actual requirements, such as height, length, width, girth.

The mathematic form of the feature curve can be defined as  $F = \{D; R; S\}$ . F denotes the feature curve. D is the set of control points. R is the constraint type illustrated in Tab. 1. S is the semantic parameter of the feature curve.

**Table 1:** Constraints of feature curves

| Constraint classification | Simple constraint (SC)          |  |  | Complex constraint (CC)  |
|---------------------------|---------------------------------|--|--|--|
|                           | Geometric constraint            | Topologic constraint   | Size constraint  | Compound constant  |
| Unitary constraint        | Self-symmetry (F <sub>1</sub> ) | Coplanar (F <sub>2</sub> )<br>Collinear (F <sub>3</sub> )                                  | Curve length (F <sub>4</sub> )                                 | Polygon constraint (F <sub>5</sub> )<br>Control point following motion (F <sub>6</sub> )<br>Self-intersection (F <sub>7</sub> )<br>Surface constraint (F <sub>8</sub> )<br>Single loop constraint (F <sub>9</sub> )<br>Double loop constraint (F <sub>10</sub> ) |
| Binary constraint         | Symmetry (F <sub>11</sub> )     | Concurrent (F <sub>12</sub> )<br>Coplanar (F <sub>13</sub> )<br>Tangent (F <sub>14</sub> ) | Size proportion (F <sub>15</sub> )<br>angle (F <sub>16</sub> ) | Quadrant constraint (F <sub>17</sub> )   |

After generation, the feature frame can be modified to get a new model. There are two ways to realize the modifications: size-driving and sketch-driving. Size-driving means to drive the target feature curve by modifying its sizes. Sketch-driving refers to driving the target feature curve by sketch interaction. During the process of driving, it is necessary to use appropriate constraint solving methods to maintain the constraints between the characteristic curves. Resultantly, a new feature frame can be generated.

Based on the feature frame, some key points are generated according to the given sizes and the parametric relations among them. On the basis of these key points, all the boundary curves of the four-sided subdomain can be obtained. If we only discuss the case in two dimension, all the subdomains denote the NURBS surfaces. The feature frame is divided into multi subdomains by adding some curves. Then all the control points of each subdomain can be acquired using the interpolation method such as Coons method. Accordingly, the parametric representation of the whole model can be finished. Thus, the relation between the size parameters and the control points can be built.

If we discuss the case in three dimension, the thing gets complicated. The first difficulty exists in the segmentation of the feature frame. Dividing the feature frame into many cube-like subdomains is far from a simple task. The second difficulty exists in the volume parameterization. Construction of volume parameterization for each subdomain is the core task of the research of parameterization and has attracted many scholars' interests. Here we only focus on the two dimensional case.

## 5 Isogeometric Analysis of Complex Model

### 5.1 Basic Formulation of IGA

If given a set of knot vectors  $[\xi_1, \xi_2, \xi_3, \dots, \xi_{n+p+1}]$ , the B-spline curve can be defined as [34],

$$C(\xi) = \sum_{i=1}^n N_{i,p}(\xi) P_i \quad (1)$$

where  $P_i$  is the set of control points.  $N_{i,p}$  is the B-spline basis function with the order  $p$ . Similarly, the B-spline surface can be defined as,

$$S(\xi, \eta) = \sum_{i=1}^n \sum_{j=1}^m N_{i,p}(\xi) N_{j,q}(\eta) P_{ij} \quad (2)$$

B-spline solid is defined as,

$$V(\xi, \eta, \zeta) = \sum_{i=1}^n \sum_{j=1}^m \sum_{k=1}^l N_{i,p}(\xi) N_{j,q}(\eta) N_{k,r}(\zeta) P_{i,j,k} \quad (3)$$

In this paper, the linear elastic problem is taken as an example for study. The principle of minimum potential energy is applied to obtain the equation of equilibrium according to relative mechanics principles and variation principles.

$$Ku = f \quad (4)$$

where  $u$  is the array of unknowns for the control points.  $f$  is the loads applied on the model.  $K$  is the stiffness matrix presented as follows,

$$K = \int_{\Omega} B^T D B d\Omega \quad (5)$$

To calculate the stiffness matrix  $K$ , three domains are defined. They are the physical domain  $\Omega$  and its subdomain or element  $\Omega_e$ , the parameter domain  $\hat{\Omega}$  and its subdomain or element  $\hat{\Omega}_e$ , and the parent domain  $\tilde{\Omega}$ , respectively. The relative mapping relations are defined as follows.  $\tilde{\phi}_e : \tilde{\Omega} \rightarrow \hat{\Omega}_e$  is the mapping from the parent domain to the parameter subdomain.  $S : \hat{\Omega}_e \rightarrow \Omega_e$  is the mapping from the parameter subdomain to the physical subdomain. Therefore, the function is  $S \circ \tilde{\phi}_e$  for mapping  $X_e : \tilde{\Omega} \rightarrow \Omega_e$  from the parent domain to the physical subdomain. For the three dimensional case, an element in the parameter space is

$\hat{\Omega}_e = [\xi_i, \xi_{i+1}] \otimes [\eta_j, \eta_{j+1}] \otimes [\zeta_k, \zeta_{k+1}]$ . Any point in parameter space  $(\xi, \eta, \zeta)$  can be expressed as follows with the point  $(\tilde{\xi}, \tilde{\eta}, \tilde{\zeta})$  by the mapping  $\tilde{\phi}_e : \tilde{\Omega} \rightarrow \hat{\Omega}_e$

$$\begin{bmatrix} \xi \\ \eta \\ \zeta \end{bmatrix} = \tilde{\phi}^e(\tilde{\zeta}) = 0.5 \times \begin{bmatrix} (\xi_{i+1} - \xi_i)\tilde{\zeta} + (\xi_{i+1} + \xi_i) \\ (\eta_{j+1} - \eta_j)\tilde{\eta} + (\eta_{j+1} + \eta_j) \\ (\zeta_{k+1} - \zeta_k)\tilde{\zeta} + (\zeta_{k+1} + \zeta_k) \end{bmatrix} \quad (6)$$

The Jacobian transformation matrix of mapping  $S : \hat{\Omega}_e \rightarrow \Omega_e$  is

$$J_1 = \begin{bmatrix} \frac{\partial x}{\partial \xi} & \frac{\partial x}{\partial \eta} & \frac{\partial x}{\partial \zeta} \\ \frac{\partial y}{\partial \xi} & \frac{\partial y}{\partial \eta} & \frac{\partial y}{\partial \zeta} \\ \frac{\partial z}{\partial \xi} & \frac{\partial z}{\partial \eta} & \frac{\partial z}{\partial \zeta} \end{bmatrix} \quad (7)$$

The Jacobian transformation determinant for the transformation from the parameter coordinate to the parent unit coordinate is

$$J_2 = \begin{bmatrix} \frac{1}{2}(\xi_{i+1} - \xi_i) & 0 & 0 \\ 0 & \frac{1}{2}(\eta_{i+1} - \eta_i) & 0 \\ 0 & 0 & \frac{1}{2}(\zeta_{i+1} - \zeta_i) \end{bmatrix} \quad (8)$$

The Jacobian determinant of mapping  $X_e : \tilde{\Omega} \rightarrow \Omega_e$  is

$$J = J_1 * J_2 \quad (9)$$

The integral form of the stiffness matrix in the whole physical space is as follows.

$$K = \sum_{e=1}^{n_{el}} \int_{\Omega_e} K_e = \sum_{e=1}^{n_{el}} \int_{\Omega_e} B_e^T D B_e d\Omega_e = \sum_{e=1}^{n_{el}} \int_{\hat{\Omega}_e} B_e^T D B_e |J_1| d\hat{\Omega}_e = \sum_{e=1}^{n_{el}} \int_{\tilde{\Omega}_e} B_e^T D B_e |J| d\tilde{\Omega}_e \quad (10)$$

where  $n_e$  is the number of the elements or subdomains. The item  $B$  is defined as follows.

$$B = [B_1 \quad B_2 \quad \cdots \quad B_s \quad \cdots \quad B_{n_e}]^T \quad (11)$$

$$B_s = \begin{bmatrix} \frac{\partial R_s}{\partial x} & 0 & 0 & \frac{\partial R_s}{\partial y} & \frac{\partial R_s}{\partial x} & 0 \\ 0 & \frac{\partial R_s}{\partial y} & 0 & 0 & \frac{\partial R_s}{\partial z} & \frac{\partial R_s}{\partial y} \\ 0 & 0 & \frac{\partial R_s}{\partial z} & \frac{\partial R_s}{\partial z} & 0 & \frac{\partial R_s}{\partial x} \end{bmatrix} \quad (12)$$

$R_s$  is defined as follows,

$$\begin{aligned}
R_s &= R_{i,p}(\xi)R_{j,q}(\eta)R_{k,r}(\zeta) \\
s &= (k-1) \times m \times n + (j-1) \times n + i, \quad 1 \leq i \leq n, 1 \leq j \leq m, 1 \leq k \leq l \\
n_e &= l \times m \times n
\end{aligned} \tag{13}$$

Then, the matrixes of strain and stress can be computed as follows,

$$\varepsilon = \frac{1}{2}(\nabla u + \nabla^T u) = Bu \tag{14}$$

$$\sigma = D\varepsilon = DBu \tag{15}$$

where,  $D$  is a constant matrix.

For the plane stress problem,  $D$  is defined as follows,

$$[D] = \frac{E}{1-\mu^2} \begin{bmatrix} 1 & \mu & 0 \\ \mu & 1 & 0 \\ 0 & 0 & \frac{1-\mu}{2} \end{bmatrix} \tag{16}$$

For the plane strain problem,  $D$  is defined as follows. Where  $E$  represents the Elastic Modulus,  $\mu$  represents Poisson's ratio.

$$[D] = \frac{E(1-\mu)}{(1+\mu)(1-2\mu)} \begin{bmatrix} 1 & \frac{\mu}{1-\mu} & 0 \\ \frac{\mu}{1-\mu} & 1 & 0 \\ 0 & 0 & \frac{1-2\mu}{2(1-\mu)} \end{bmatrix} \tag{17}$$

## 5.2 IGA for Multi-Patches

One model can be divided into many subdomains. The whole interface curve is shared by two subdomains. The equation of equilibrium for each subdomain is integrated into the global equation of equilibrium. By solving the equation, the analysis of the whole structure is realized. If the two subdomains don't share the same interface curve, a connectivity matrix is imported to establish a correspondence between the two subdomains. The following derivation is in accordance with the subdomains with the same interface curve [38].

Considering a plane linear elastic with a region  $\Omega$ , the region  $\Omega$  is divided into  $r$  non-overlapping regions  $\Omega^m$  ( $m = 1, 2, \dots, r$ ). Suppose  $r = 2$ ,  $\Omega = \Omega^1 \cap \Omega^2$ , as shown in Fig. 4.

$$\begin{aligned}
-\nabla \sigma^m &= b^m && \text{in } \Omega^m \\
\sigma^m \cdot n^m &= \bar{t}^m && \text{on } S_\sigma^m \\
u^m &= \bar{u}^m && \text{on } S_u^m \\
\sigma^1 \cdot n^1 &= -\sigma^2 \cdot n^2 && \text{on } S^* \\
\bar{u}^1 &= \bar{u}^2 && \text{on } S^*
\end{aligned} \tag{18}$$

where  $u^m$  denotes the unknown displacement field.  $\sigma^m$  denotes the stress tensor.  $b^m$  denotes volume force.  $\bar{t}^m$  and  $\bar{u}^m$  are the external traction and the displacement respectively for the boundary  $S^m$  that is composed of  $S_\sigma^m$  and  $S_u^m$ .  $n^m$  is the outward unit normal of  $S^m$ . The last two equations ensure the continuity of traction and

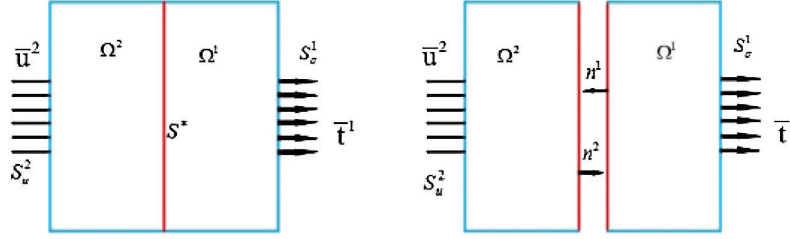


**Figure 4:** Decomposition of the solution domain

displacement of boundary  $S^*$ .  $n^1$  and  $n^2$  are the outward unit normal of  $\Omega^1$  and  $\Omega^2$  respectively. According to the method [38], the stiffness matrix in multiple patches is expressed as:

$$K = K^b + K^n + (K^n)^T + K^s \quad (19)$$

The relevant stiffness matrix is given by:

$$K^b = \sum_{m=1}^2 \int_{\Omega^m} (B^m)^T D^m B^m d\Omega^m \quad (20)$$

$$K^n = \begin{bmatrix} -\chi \int_{S^*} (R^1)^T n D^1 B^1 dS & -(1 - \chi) \int_{S^*} (R^1)^T n D^2 B^2 dS \\ \chi \int_{S^*} (R^2)^T n D^1 B^1 dS & (1 - \chi) \int_{S^*} (R^2)^T n D^2 B^2 dS \end{bmatrix} \quad (21)$$

$$K^s = \begin{bmatrix} \int_{S^*} \alpha (R^1)^T R^1 dS & - \int_{S^*} \alpha (R^1)^T R^2 dS \\ - \int_{S^*} \alpha (R^2)^T R^1 dS & \int_{S^*} \alpha (R^2)^T R^2 dS \end{bmatrix} \quad (22)$$

$R_{ij}^m(\xi, \eta)$  is a binary NURBS basis function supporting the  $m$ th patches  $\hat{\Omega} = [\xi_1, \xi_{n+p+1}] \times [\eta_1, \eta_{m+p+1}]$ .

$$R_{ij}(\xi, \eta) = N_{i,p}(\xi) N_{j,q}(\eta) \quad (23)$$

The force vector  $f$  is expressed as

$$f = \sum_{m=1}^2 \int_{\Omega^m} (R^m)^T b^m d\Omega + \sum_{m=1}^2 \int_{S_u^m} (R^m)^T \bar{t}^m dS \quad (24)$$

Substitute Eqs. (19) and (24) into Eq. (4), we can get the equation of equilibrium for the whole domain. By solving the equation, we can get the matrix of displacement  $u$  for each patch. If the number of subdomain is more than two, the relevant matrices of stiffness and load are listed here.

$$\begin{aligned}
K^b &= \sum_{ph=1}^{nph} \int_{\Omega^{ph}} (B^{ph})^T D^{ph} B^{ph} d\Omega^{ph} \\
K^n &= \begin{bmatrix} -\chi \sum_{ph=1}^{nph-1} \int_{S^*} (R^{ph})^T n D^{ph} B^{ph} dS & -(1-\chi) \sum_{ph=2}^{nph-1} \int_{S^*} (R^{ph-1})^T n D^{ph} B^{ph} dS \\ \chi \sum_{ph=1}^{nph-1} \int_{S^*} (R^{ph+1})^T n D^{ph} B^{ph} dS & (1-\chi) \sum_{ph=2}^{nph-1} \int_{S^*} (R^{ph})^T n D^{ph} B^{ph} dS \end{bmatrix} \\
K^s &= \begin{bmatrix} \sum_{ph=1}^{nph-1} \int_{S^*} \alpha (R^{ph})^T R^{ph} dS & - \sum_{ph=2}^{nph-1} \int_{S^*} \alpha (R^{ph-1})^T R^{ph} dS \\ - \sum_{ph=1}^{nph-1} \int_{S^*} \alpha (R^{ph+1})^T R^{ph} dS & \sum_{ph=2}^{nph-1} \int_{S^*} \alpha (R^{ph})^T R^{ph} dS \end{bmatrix} \\
f &= \sum_{ph=1}^{nph} \int_{\Omega^{ph}} (R^{ph})^T b^{ph} d\Omega + \sum_{ph=1}^{nph} \int_{S_\sigma^{ph}} (R^{ph})^T \bar{t}^{ph} dS
\end{aligned} \tag{25}$$

where  $ph$  denotes the index of the subdomain,  $nph$  is the total number of all the subdomains.

## 6 Structural Optimization

### 6.1 Optimization Principle

For the linear elastic problem, the single object of structure optimization is usually to minimize the volume or the area of the structure [39–41]. There are two optimization function. The objective function  $\psi_1$  is represented for the flexibility of the model by the formula  $\psi_1([\beta_i]) = f^T u$ . The objective function  $\psi_2$  is represented for the von Mises stress by the formula  $\psi_2([\alpha_j]) = \sigma_{von}$ . The design variables  $\beta_i$  is the feature sizes, and  $\alpha_j$  is the coordinate component of control points to be optimized. In two dimensional case, there are two coordinate components denoting  $x$  and  $y$ . All the coordinate components of the optimized control points are arranged into a linear set  $\{\alpha_j\}$ .

$$\min \psi_1([\beta_i]) = f^T u$$

$$\begin{aligned}
st. \quad \psi_2([\alpha_j]) &= \sqrt{\frac{\sigma_{xx}^2 + \sigma_{yy}^2 + (\sigma_{xx} - \sigma_{yy})^2 + 6\sigma_{xy}^2}{2}} \\
V &\leq V^*
\end{aligned} \tag{26}$$

$$Ku = f$$

$$[\alpha_j]_{\min} \leq [\alpha_j] \leq [\alpha_j]_{\max}$$

$$[\beta_i]_{\min} \leq [\beta_i] \leq [\beta_i]_{\max}$$

### 6.2 Derivation of Sensitivity Matrix

The derivative of objective function in the formula (26) with respect to  $\alpha_i$  needs to be calculated.

$$\frac{d\psi_1}{d\beta_i} = \frac{d(f^T u)}{d\beta_i} = \frac{df^T}{d\beta_i} u + f^T \frac{du}{d\beta_i} \tag{27}$$

Since the load vector is independent of  $\beta_i$ , so  $\frac{df^T}{d\beta_i} = 0$ . Thus the first item of the formula (27) is eliminated and the following formula comes out.

$$\frac{d\psi_1}{d\beta_i} = f^T \frac{du}{d\beta_i} \quad (28)$$

To calculate the formula (28), the item  $\frac{du}{d\beta_i}$  is required to compute. From the equation of equilibrium  $Ku = f$ , we can get the formula (29) by deriving the equation on both sides of it. The formula (30) is also obtained by transposing the item.

$$\frac{dK}{d\beta_i} u + K \frac{du}{d\beta_i} = 0 \quad (29)$$

$$\frac{du}{d\beta_i} = -K^{-1} \frac{dK}{d\beta_i} u \quad (30)$$

Taking the formula (30) into the formula (28), we can get the following formula since the matrix  $K$  is symmetric.

$$\frac{d\psi_1}{d\beta_i} = f^T \frac{du}{d\beta_i} = -f^T K^{-1} \frac{dK}{d\beta_i} u = -u^T K^T K^{-1} \frac{dK}{d\beta_i} u = -u^T \frac{dK}{d\beta_i} u \quad (31)$$

According to the chain rule of derivation, we can get,

$$\frac{d\psi_1}{d\beta_i} = -u^T \frac{dK}{d\alpha_j} \cdot \frac{d\alpha_j}{d\beta_i} u$$

According to the definition of  $\alpha_j$ , the item  $\frac{d\alpha_j}{d\beta_i}$  can be written as  $\frac{d[P_{j,x} \ P_{j,y}]}{d\beta_i}$ . Since we have constructed the relation between the control points and the feature sizes in Section 4.2, the item  $\frac{d\alpha_j}{d\beta_i}$  can be derived from the parametric representation of each subdomain.

For another object function,

$$\frac{d\psi_2}{d\alpha_j} = \frac{d\sigma_{von}}{d\alpha_j} \quad (32)$$

If defining  $\hat{\sigma} = [\sigma_{xx} \ \sigma_{yy} \ \sigma_{xx} - \sigma_{yy} \ \sqrt{6} \sigma_{xy}]$ , we can get  $\sigma_{von} = \sqrt{\hat{\sigma} \hat{\sigma}^T} / 2$  and then get the sensitivity matrix according to the partial derivative of  $\sigma_{von}$  with respect to  $\alpha_j$ .

$$\frac{d\sigma_{von}}{d\alpha_j} = \frac{1}{\sqrt{2\hat{\sigma} \hat{\sigma}^T}} \hat{\sigma} \frac{d\hat{\sigma}}{d\alpha_j} \quad (33)$$

If introducing a matrix  $A$ ,  $\hat{\sigma}$  can also be written as the following matrix.

$$\hat{\sigma}^T = \begin{bmatrix} 1 & 0 & 0 \\ 0 & 1 & 0 \\ 1 & -1 & 0 \\ 0 & 0 & \sqrt{6} \end{bmatrix} [\sigma_{xx} \ \sigma_{yy} \ \sigma_{xy}]^T = A\sigma^T \quad (34)$$

If defining  $C = A^T A$ , we can get following formula since  $\sigma = [\sigma_{xx} \ \sigma_{yy} \ \sigma_{xy}] = DBu$ .

$$\frac{d\sigma_{von}}{d\alpha_j} = \frac{1}{\sqrt{2\sigma C\sigma}} \sigma C \frac{d(\sigma^T)}{d\alpha_j} = \frac{1}{\sqrt{2\sigma C\sigma}} \sigma CDB \frac{du^T}{d\alpha_j} \quad (35)$$

Taking the formula into the Eq. (33), we can get

$$\frac{d\sigma_{von}}{d\alpha_j} = -\frac{\sigma CDB}{\sqrt{2\sigma C\sigma}} (K^{-1} \frac{dK}{d\alpha_j} u)^T \quad (36)$$

Calculating both  $\frac{d\psi_1}{d\alpha_j}$  and  $\frac{d\psi_2}{d\alpha_j}$  requires to solve  $\frac{dK}{d\alpha_j}$ . For  $K = K^b + K^n + (K^n)^T + K^s$ , we should firstly get  $\frac{\partial K^b}{\partial \alpha_j}, \frac{\partial K^n}{\partial \alpha_j}, \frac{\partial K^s}{\partial \alpha_j}$ . The problem is further deduced as  $\frac{\partial K_e^b}{\partial \alpha_j}, \frac{\partial K_e^n}{\partial \alpha_j}, \frac{\partial K_e^s}{\partial \alpha_j}$  since  $K^b, K^n, K^s$  are all assembled by  $K_e^b, K_e^n, K_e^s$ . The design variable  $\alpha_j$  is not included in  $K_e^s$ , so  $\frac{\partial K_e^s}{\partial \alpha_j}$  will vanishes.

$$\begin{aligned} \frac{\partial K_e^b}{\partial \alpha_j} &= \sum_{m=1}^2 \left( \int_{\Omega^m} \frac{\partial (B_e^m)^T}{\partial \alpha_j} D^m B_e^m |J^m| d\Omega^m + \int_{\Omega^m} (B_e^m)^T D^m \frac{\partial B_e^m}{\partial \alpha_j} |J^m| d\Omega^m \right. \\ &\left. + \int_{\Omega^m} (B_e^m)^T D^m B_e^m \frac{\partial |J^m|}{\partial \alpha_j} d\Omega^m \right) \end{aligned} \quad (37)$$

$$\frac{\partial K_e^n}{\partial \alpha_j} = \begin{bmatrix} \frac{\partial K_e^{n,11}}{\partial \alpha_j} & \frac{\partial K_e^{n,12}}{\partial \alpha_j} \\ \frac{\partial K_e^{n,21}}{\partial \alpha_j} & \frac{\partial K_e^{n,22}}{\partial \alpha_j} \end{bmatrix} = \frac{1}{2} \times \begin{bmatrix} -\int_{S_e^*} (R^1)^T nD^1 \frac{\partial B_e^1}{\partial \alpha_j} dS & -\int_{S_e^*} (R^1)^T nD^2 \frac{\partial B_e^2}{\partial \alpha_j} dS \\ \int_{S_e^*} (R^2)^T nD^1 \frac{\partial B_e^1}{\partial \alpha_j} dS & \int_{S_e^*} (R^2)^T nD^2 \frac{\partial B_e^2}{\partial \alpha_j} dS \end{bmatrix} \quad (38)$$

When calculating  $\frac{\partial K_e^n}{\partial \alpha_j}, \frac{\partial K_e^s}{\partial \alpha_j}$ , we need to integrate along the curve S. Under the premise of ensuring the continuity of the sub-patches, the Gaussian integral of the linear element can be used to solve the interface integral, that is to calculate the sum of the integrand which is transformed by the curve  $S^*$ .

$$\frac{\partial K_e^{n,11}}{\partial \alpha_j} = -\frac{1}{2} \times \int_{S_e^*} (R^1)^T nD^1 \frac{\partial B_e^1}{\partial \alpha_j} dS = -\sum_{i=1}^{ngp} (R^1)^T nD^1 \frac{\partial B_e^1}{\partial \alpha_j} w_i \quad (39)$$

In the formula,  $ngp$  denotes the number of Gaussian integration points, and  $w_i$  is the weight.

$$\frac{\partial K_e^n}{\partial \alpha_j} = \frac{1}{2} \times \begin{bmatrix} -\sum_{i=1}^{ngp} (R^1)^T nD^1 \frac{\partial B_e^1}{\partial \alpha_j} w_i & \sum_{i=1}^{ngp} (R^1)^T nD^2 \frac{\partial B_e^2}{\partial \alpha_j} w_i \\ \sum_{i=1}^{ngp} (R^2)^T nD^1 \frac{\partial B_e^1}{\partial \alpha_j} w_i & \sum_{i=1}^{ngp} (R^2)^T nD^2 \frac{\partial B_e^2}{\partial \alpha_j} w_i \end{bmatrix} \quad (40)$$

In the above formula, the items of  $\frac{\partial B_e^m}{\partial \alpha_j}$  and  $\frac{\partial |J^m|}{\partial \alpha_j}$  should be derived. In order to calculate these two items, two matrices are defined in the first place.

Derivative on both sides of Eq. (11):

$$\frac{\partial B_e^m}{\partial \alpha_j} = \frac{\partial [B_1^m \ B_2^m \ \cdots \ B_s^m \ \cdots \ B_{n_e}^m]}{\partial \alpha_j} \quad (41)$$

According to Eq. (12):

$$B_s = \begin{bmatrix} \frac{\partial R_s}{\partial x} & 0 & 0 \\ 0 & \frac{\partial R_s}{\partial y} & \frac{\partial R_s}{\partial y} \\ 0 & 0 & \frac{\partial R_s}{\partial x} \end{bmatrix} \quad (42)$$

We can get Eq. (43) by substituting Eq. (42) into Eq. (11):

$$B_e^m = \begin{bmatrix} R_{1,x} & 0 & 0 & R_{2,x} & 0 & 0 & \cdots & R_{n_e,x} & 0 & 0 \\ 0 & R_{1,y} & R_{1,y} & 0 & R_{2,y} & R_{2,y} & \cdots & 0 & R_{n_e,y} & R_{n_e,y} \\ 0 & 0 & R_{1,x} & 0 & 0 & R_{2,x} & \cdots & 0 & 0 & R_{n_e,x} \end{bmatrix} \quad (43)$$

Two matrices  $T_e^m, \hat{T}_e^m$  can be defined by elements of  $B_e^m$ .  $B_e^m$  can be obtained by  $T_e^m$  through element transformation, and  $\hat{T}_e^m$  can be obtained by mapping transformation of  $T_e^m$ .

$$T_e^m = \begin{bmatrix} R_{1,x} & R_{1,y} \\ R_{2,x} & R_{2,y} \\ \vdots & \vdots \\ R_{n_e,x} & R_{n_e,y} \end{bmatrix} \quad \hat{T}_e^m = \begin{bmatrix} R_{1,\xi} & R_{1,\eta} \\ R_{2,\xi} & R_{2,\eta} \\ \vdots & \vdots \\ R_{n_e,\xi} & R_{n_e,\eta} \end{bmatrix} \quad (44)$$

According to Eq. (7):

$$J_1^m = \begin{bmatrix} \frac{dx}{d\xi} & \frac{dx}{d\eta} \\ \frac{dy}{d\xi} & \frac{dy}{d\eta} \end{bmatrix} \quad (45)$$

We can get,

$$\hat{T}_e^m = J_1^m T_e^m \quad (46)$$

If the formula (3) is written into a matrix formation, we can get the following expression for one calculating element.

$$V_e^m(\xi, \eta) = \begin{bmatrix} x \\ y \end{bmatrix} = (P_e^m)^T R_e^m \quad (47)$$

where  $R_e^m = [R_1 \ R_2 \ \cdots \ R_s \ \cdots \ R_{n_e}]^T$  and  $R_s$  have been defined in the formula (13).  $P_e^m$  is the coordinate matrix of all the control points in a calculating element.

$$P_e^m = \begin{bmatrix} x_1 & x_2 & \cdots & x_{n_e} \\ y_1 & y_2 & \cdots & y_{n_e} \end{bmatrix} \quad (48)$$

On derivate of the formula (47) on both sides, we can get the formula (49).

$$\left[ \frac{\partial V_e^m}{\partial \xi} \quad \frac{\partial V_e^m}{\partial \eta} \right] = \left[ \frac{\partial R_e^m}{\partial \xi} \quad \frac{\partial R_e^m}{\partial \eta} \right] P_e^m + R_e^m \left[ \frac{\partial P_e^m}{\partial \xi} \quad \frac{\partial P_e^m}{\partial \eta} \right] \quad (49)$$

The second item after the equal-sign of the formula (49) is equal to zero. According to the definition of  $\hat{T}$ , the following formula can be derived.

$$J_1^m = \hat{T}_e^m P_e^m \quad (50)$$

On the derivate of the formula (46) and the formula (50) on both sides respectively, we can get the formula (51).

$$\frac{\partial T_e^m}{\partial \alpha_j} = -T_e^m \frac{\partial J_1^m}{\partial \alpha_j} (J_1^m)^{-1} = -T_e^m \frac{\partial (P_e^m)^T}{\partial \alpha_j} \hat{T}_e^m (J_1^m)^{-1} = -T_e^m \frac{\partial (P_e^m)^T}{\partial \alpha_j} T_e^m \quad (51)$$

According to the definitions of the matrices B and T, which are defined in the formula (11) and (43) respectively, we can get  $\frac{\partial B_e^m}{\partial \alpha_j}$  by rearranging the non-zero items of  $\frac{\partial T_e^m}{\partial \alpha_j}$ .

Next,  $\frac{\partial |J_e^m|}{\partial \alpha_j}$  is calculated. To avoid confusion with the parameter of  $J_2$ , the parameter of  $\alpha_j$  is written into the form  $\alpha_p$  since there is no relationship between them.

$$\frac{\partial P_e^m}{\partial \alpha_j} = \begin{bmatrix} \frac{\partial x_1}{\partial \alpha_j} & \frac{\partial y_1}{\partial \alpha_j} \\ \frac{\partial x_2}{\partial \alpha_j} & \frac{\partial y_2}{\partial \alpha_j} \\ \vdots & \vdots \\ \frac{\partial x_{ne}}{\partial \alpha_j} & \frac{\partial y_{ne}}{\partial \alpha_j} \end{bmatrix} \quad (52)$$

According to formula (13), formula (53) is obtained:

$$J_2^m = \begin{bmatrix} \frac{1}{2}(\xi_{i+1} - \xi_i) & 0 \\ 0 & \frac{1}{2}(\eta_{j+1} - \eta_i) \end{bmatrix} \quad (53)$$

And we can get the following equation based on Eq. (15):

$$|J_e^m| = |J_1^m| |J_2^m| \quad (54)$$

Taking the derivative of both sides of formula (53) to get formula (55):

$$\begin{aligned} \frac{\partial |J_e^m|}{\partial \alpha_j} &= \frac{\partial (|J_1^m| \cdot |J_2^m|)}{\partial \alpha_j} = |J_2^m| \cdot \frac{\partial (|J_1^m|)}{\partial \alpha_j} \\ &= |J_2^m| \cdot |J_1^m| \cdot \text{tr} \left( (J_1^m)^{-1} \frac{\partial J_1^m}{\partial \alpha_j} \right) = |J_2^m| \cdot |J_1^m| \cdot \text{tr} \left( (J_1^m)^{-1} \frac{\partial (P_e^m)^T}{\partial \alpha_j} M^m \right) \\ &= |J_2^m| \cdot |J_1^m| \cdot \text{tr} \left( (J_1^m)^{-1} M^m \frac{\partial (P_e^m)^T}{\partial \alpha_j} \right) = |J_e^m| \cdot \text{tr} \left( \Gamma^m \frac{\partial (P_e^m)^T}{\partial \alpha_j} \right) \end{aligned} \quad (55)$$

where  $\text{tr}(Z)$  denotes the sum of the diagonal elements of  $Z$ . The load applied on the model is independent of the design variable, so the derivative of the element load array F to the design variables is 0, i.e.,  $\frac{\partial f_e}{\partial \alpha_j} = 0$ . By the

above Eqs. (51) and (55), we can learn  $\frac{\partial B_e^m}{\partial \alpha_j}$  and  $\frac{\partial |J_e^m|}{\partial \alpha_j}$ .

Bringing these two data into Eqs. (36), (37) and (39), we are able to respectively calculate  $\frac{\partial k_e^b}{\partial \alpha_j}$  which is the derivative of element volume matrix to design variable,  $\frac{\partial k_e^n}{\partial \alpha_j}$  and  $\frac{\partial k_e^s}{\partial \alpha_j}$  are the derivatives of the element coupling matrix to design variables.

Optimization algorithm is the key technology that influences the quality and efficiency of shape optimization. This paper employs the method of moving asymptotes called MMA [36]. The MMA algorithm is used to update the design variables in each iterative step by using the sensitivity matrix.

## 7 Examples and Discussions

We select two planar complex models to verify our method. The first is a connecting-rod and the second is a load-bearing part. In the two examples, the elasticity modulus  $E$  is equal to  $1e5$  and the Poisson's ratio  $\nu$  is equal to  $0.3$ . Since the constraints of each model are not same, a general feature frame model cannot be given. The size optimization is performed directly on the feature frame model with the objective of flexibility by taking the size parameters as design variables. Based on the result of the size optimization, shape optimization is realized with the objective of equivalent stress by taking the control points as the design variables.

### 7.1 Example 1: Optimization of Connecting-Rod

The connecting-rod model has 9 size parameters. The feature frame model is constructed according to these size parameters, as shown in Fig. 5a. After adding some auxiliary curves, the feature frame model is subdivided into 12 sub-patches. Each sub-patch is interpolated as NURBS surfaces, as shown in Fig. 5b. The degree of the 12 sub-patches is equal to 2 in both parameter directions of  $U$  and  $V$ , and the knot vectors in the two parameter directions are  $\{0,0,0,1,1,1\}$ . Giving all the parametric equations is a tedious work, so we select some key points and give the equations of them. All the parameters in the equations are denoted in Fig. 5a. Then, all the control points of all the subdomains can be obtained using the Coons method on the basis of these key points. The constraints listed in the Tab. 1 are applied on the parametric model, such as the geometric constraint F1 and F11, the topologic constraint F3 and F14, the size constraint F4. Since parametric design for 2D model is not a complex work, we will not give the detail here.

$$\begin{aligned}
 P_1 &= \begin{bmatrix} x_1 \\ y_1 \end{bmatrix} = \begin{bmatrix} -1R1 + 0R2 \cdots 0L2 \\ 0R1 + 0R2 \cdots 0L2 \end{bmatrix} = \begin{bmatrix} -R1 \\ 0 \end{bmatrix} \\
 P_2 &= \begin{bmatrix} x_2 \\ y_2 \end{bmatrix} = \begin{bmatrix} 0R1 + 0R2 + \cdots \frac{1}{2}L5 + \cdots 0L2 \\ 0R1 + 0R2 + \cdots L3 \cdots 0L2 \end{bmatrix} = \begin{bmatrix} \frac{1}{2}L5 \\ L3 \end{bmatrix} \\
 P_3 &= \begin{bmatrix} x_3 \\ y_3 \end{bmatrix} = \begin{bmatrix} 0R1 + 0R2 + \cdots 1L5 + \cdots 0L2 \\ 0R1 + 1R2 + \cdots 0L2 \end{bmatrix} = \begin{bmatrix} L5 \\ R2 \end{bmatrix} \\
 P_4 &= \begin{bmatrix} x_4 \\ y_4 \end{bmatrix} = \begin{bmatrix} 0R1 + 0R2 + \cdots 1L1 + 1L5 \cdots 0L2 \\ 0R1 + 0R2 + \cdots -1R5 \cdots 0L2 \end{bmatrix} = \begin{bmatrix} L1 + L5 \\ -R5 \end{bmatrix} \\
 P_5 &= \begin{bmatrix} x_5 \\ y_5 \end{bmatrix} = \begin{bmatrix} 0R1 + 0R2 + \cdots 1L1 + 1L5 + \frac{1}{2}(L2 - L1) \cdots 0L2 \\ 0R1 + 0R2 + \cdots -1L4 \cdots 0L2 \end{bmatrix} = \begin{bmatrix} \frac{1}{2}(L1 + L2) + L5 \\ -L4 \end{bmatrix}
 \end{aligned}$$

The two distributed load  $P1 = 100$  N and  $P2 = 100$  N are applied to the center of the right hole. Full constraint is applied to the left hole. The objective of optimization is to minimize the global flexibility and local equivalent stress of the structure. Optimization functions consists of two functions. The first is

$\psi_1([P_i]) = f^T u$  and the second is  $\psi_2([P_i]) = \sqrt{\frac{\sigma_{xx}^2 + \sigma_{yy}^2 + (\sigma_{xx} - \sigma_{yy})^2 + 6\sigma_{xy}^2}{2}}$ . During the optimization process, the area of the model is less than a given value and the rules of the Elasticity.

A global flexibility optimization is performed, then an optimization of the local equivalent stress is applied. As shown in Figs. 6a and 6b, in the case of  $V \leq V_0 = 371$ , the flexibility is 610 and 507 before and after optimization. As shown in Fig. 6c, the maximum equivalent stress before optimization is at the slot. The slot is in a state of stress concentration with the value 4300. While in Fig. 6e, the maximum equivalent stress is cut down to 3700. The optimization efficiency reaches 16%, with the area decreasing and the stress concentration disappearing. The iteration process of objective functions is shown in Fig. 7. The size parameters before and after optimization are shown in Tab. 2.

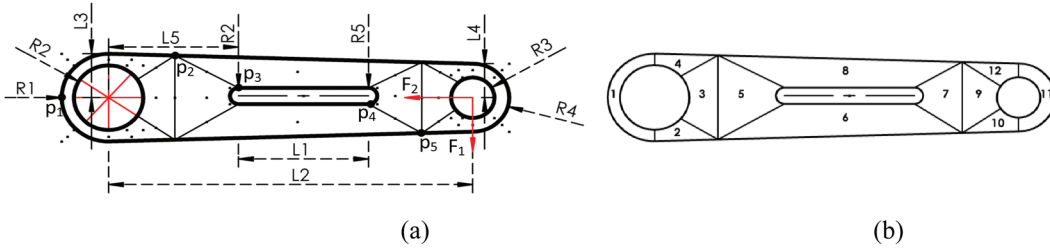


**Figure 5:** Connecting-rod. (a) The feature frame model with constraints and loads. (b) Layout of sub-patches

## 7.2 Example 2: Optimization of Load-Bearing Part

The second example is a load-bearing part from a planar flexible mechanism. As shown in Fig. 8a, the constraints and loads are imposed the parametric model, and the layout of the sub-patches that amount to 34 is displayed in Fig. 8b. The degree of these sub-patches is 2 in both U and V parameter direction. The knot vectors in the two parameter directions are  $\{0, 0, 0, 1, 1, 1\}$ . Similar with the first example, we select some key points to give the formulation of them and then get the parametric representation of all the subdomains.

The constraints is also applied on the model, such as F11, F14 and F4. Fixed displacement constraints are applied in three places depicted in the figure. The applied point load F is equate to 1000N. The target of optimization is minimization of the flexibility  $\psi_1([P_i]) = f^T u$  and the equivalent stress

$\psi_2([P_i]) = \sqrt{\frac{\sigma_{xx}^2 + \sigma_{yy}^2 + (\sigma_{xx} - \sigma_{yy})^2 + 6\sigma_{xy}^2}{2}}$  with the constraint of the area and the rules of the Elasticity.

$$P_1 = \begin{bmatrix} x_1 \\ y_1 \end{bmatrix} = \begin{bmatrix} 0a1 + 0a2 + \dots 0L2 \\ 0a1 + 0a2 + \dots 1d + 2e + 1f1 + 1g \dots 0L2 \end{bmatrix} = \begin{bmatrix} 0 \\ d + 2e + f1 + g \end{bmatrix}$$

$$P_2 = \begin{bmatrix} x_2 \\ y_2 \end{bmatrix} = \begin{bmatrix} 1a1 + 1a2 + \dots 0h2 \\ 0a1 + 0a2 + \dots 1d + 1e + 1f2 + \dots 0h2 \end{bmatrix} = \begin{bmatrix} a1 + a2 \\ d + e + f2 \end{bmatrix}$$

$$P_3 = \begin{bmatrix} x_3 \\ y_3 \end{bmatrix} = \begin{bmatrix} 1a1 + 1a2 - R1 + \dots 0h2 \\ 0a1 + 0a2 + \dots 1d + \frac{1}{2}e + \dots 0h2 \end{bmatrix} = \begin{bmatrix} a1 + a2 - R1 \\ d + \frac{1}{2}e \end{bmatrix}$$

From the result presented in the Fig. 9, the flexibility is 4721 and 3800 before and after optimization with the area constraint  $V \leq V_0 = 862$ . The optimized rate was 19%. The optimization of equivalent stress follows the size optimization. As seen in the Fig. 9c, the ring groove notch has the most severe stress concentration with the value 32483. In Fig. 9e, the maximum equivalent stress is reduced after optimization with the

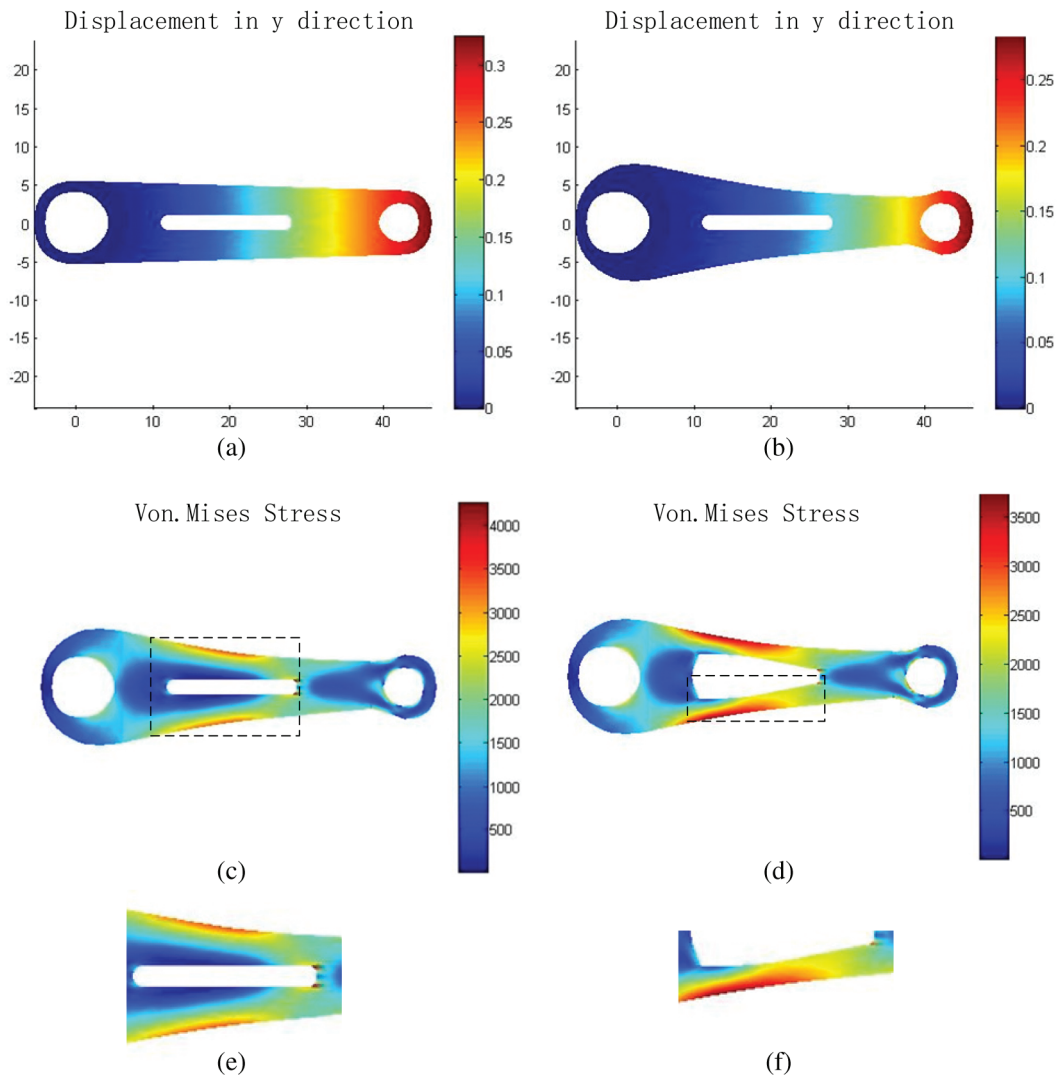


**Figure 6:** Optimization result of Connecting-rod. (a) Cloud chart of displacement in Y direction before optimization. (b) Cloud chart of displacement in Y direction after optimization. (c) Cloud chart of equivalent stress before optimization. (d) Cloud chart of equivalent stress after optimization. (e) Partially enlarged figure for the area in (c) enclosed by the dotted line. (f) Partially enlarged figure for the area in (d) enclosed by the dotted line

value 24175. The optimization efficiency of stress concentration is 29%. The iterative process of the objective function is shown in Fig. 10. The parameters of the parametric load-bearing model before and after optimization are shown in Tab. 3.

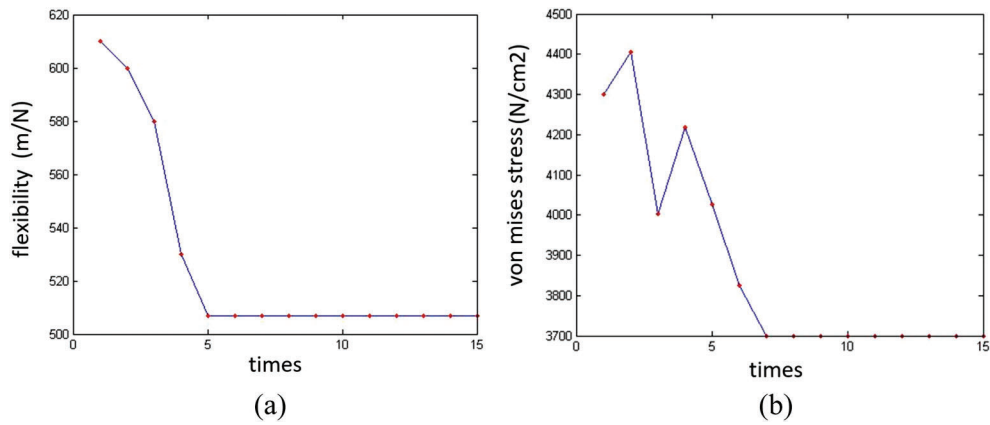


**Figure 7:** Iterative process. (a) Optimization of flexibility. (b) Optimization of equivalent stress

**Table 2:** Dimensions before and after optimization of the connecting-rod model

| Name of parameters | Before optimization | After optimization |
|--------------------|---------------------|--------------------|
| R1                 | 5.42                | 7.42               |
| R2                 | 4                   | 4                  |
| R5                 | 1                   | 1                  |
| L1                 | 15                  | 15                 |
| L2                 | 42                  | 42                 |
| L3                 | 5.13                | 5.267              |
| L4                 | -4.33               | -2.83              |
| R6                 | 1                   | 3                  |
| R3                 | 5                   | 5                  |
| R4                 | 4.2                 | 2.8                |

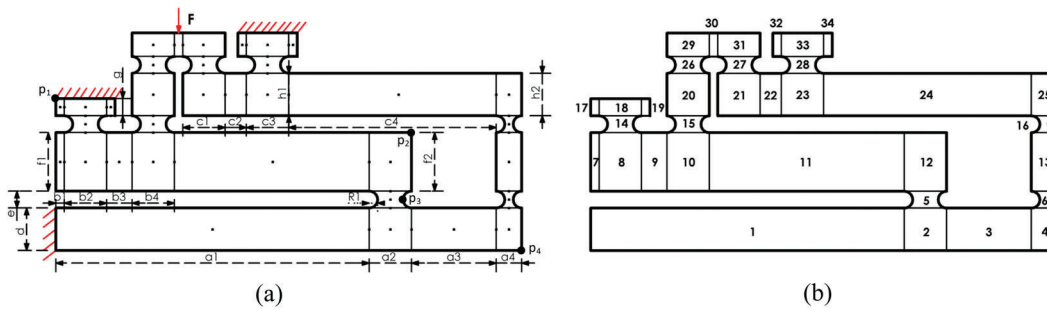


**Figure 8:** Model of load-bearing model. (a) Dimensions of the load-bearing model. (b) Sub-patches layout

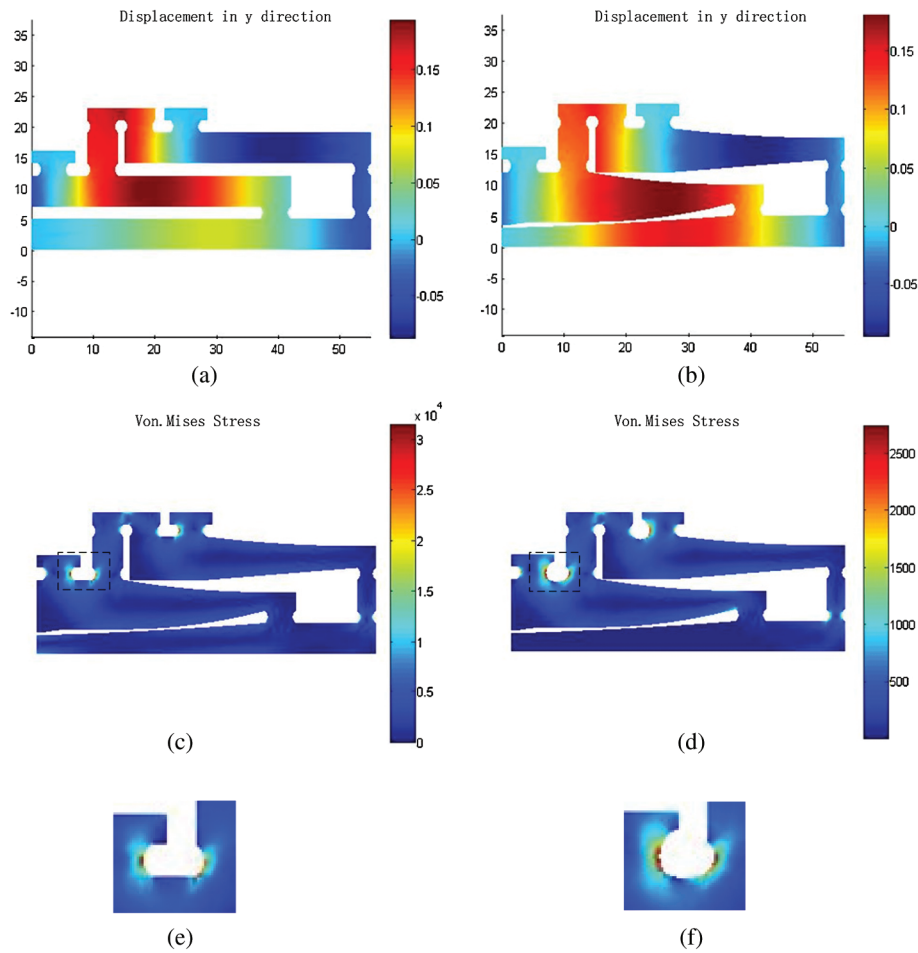


**Figure 9:** Optimization result of load-bearing part. (a) Cloud chart of displacement in Y direction before optimization. (b) Cloud chart of displacement in Y direction after optimization. (c) Cloud chart of equivalent stress before optimization. (d) Cloud chart of equivalent stress after optimization. (e) Partially enlarged figure for the area in (c) enclosed by the dotted line. (f) Partially enlarged figure for the area in (d) enclosed by the dotted line

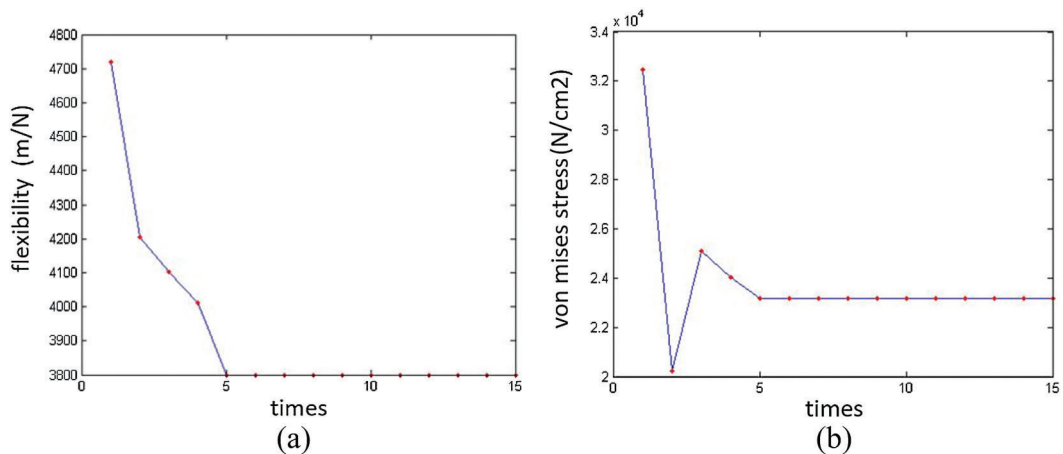


**Figure 10:** Iterative process. (a) For flexibility optimization. (b) For Equivalent stress optimization

**Table 3:** Dimensions before and after optimization of the load-bearing mode

| Name of parameters | Before optimization (mm) | After optimization (mm) |
|--------------------|--------------------------|-------------------------|
| a                  | 55                       | 55                      |
| b                  | 42                       | 42                      |
| c                  | 37                       | 37                      |
| d                  | 5                        | 2.13                    |
| e                  | 2                        | 2                       |
| f1                 | 5                        | 7.52                    |
| f2                 | 5                        | 3.17                    |
| g                  | 2                        | 0.4                     |
| h1                 | 5                        | 6.9                     |
| h2                 | 5                        | 3.21                    |

## 8 Conclusions

Our method has several advantages. The method combines the parametric design method with the isogeometric analysis. By constructing the relationship chain between design size parameters, control points and physical performance parameters, the feature frame model is used to control the overall and details of the shape. This allows the user to edit the product model through a few feature size parameters. This also avoids the complex modeling operations caused by traditional shape optimization using finite element nodes as design variables. Thus the parametric modeling and optimization are unified together.

Benefit from the parametric design, our method lightens the burden on the designer and transfer the designer's special attention from mesh operation during the stage of analysis and optimization to the creative design itself. The designers will put their attentions on optimization of the key part sizes, without taking into account nonsignificant sizes. It will be easier and more accurate to capture the designer's design intent, since it is a very important thing for computer-aided design software or computer-aided engineering software.

Thirdly, the computation efficiency is significantly improved for the variables of design and optimization are greatly reduced. In the design process, the interactions among the model of design, analysis and optimization are more convenient. This greatly reduces the product research period. Due to the B-spline basis function, the sensitivity matrix is easily acquired because the entire model has complete continuity.

It must be mentioned that the feature frame models presented in this paper is simple, so the constraints between the feature curves are single and simple as well. Meanwhile, the Coons does not always work well if the subdomains are not divided well when the model is complex. Henceforth, the next work is to construct the feature frame model with complex feature elements and constraints. More volume parameterization methods can also be applied onto the model. Thus, our method will be able to treat the more complex optimization problem.

**Acknowledgement:** Thank all the anonymous reviewers for their valuable comments and suggestions.

**Funding Statement:** This work is supported by the National Nature Science Foundation of China (No. 51475309).

**Conflicts of Interest:** The authors declare that they have no conflicts of interest to report regarding the present study.

## References

1. Bendsøe, M. P., Kikuchi, N. (1988). Generating optimal topologies in structural design using a homogenization method. *Computer Methods in Applied Mechanics & Engineering*, 71(2), 197–224. DOI 10.1016/0045-7825(88)90086-2.
2. Bendsøe, M. P., Sigmund, O. (2003). *Topology optimization: theory, methods, and applications*. Berlin Heidelberg: Springer Verlag.
3. Sigmund, O., Petersson, J. (1998). Numerical instabilities in topology optimization: a survey on procedures dealing with checkerboards, mesh-dependencies and local minima. *Structural and Multidisciplinary Optimization*, 16(1), 68–75. DOI 10.1007/BF01214002.
4. Qian, X. (2013). Topology optimization in B-spline space. *Computer Methods in Applied Mechanics and Engineering*, 265, 15–35. DOI 10.1016/j.cma.2013.06.001.
5. Klarbring, A. (2008). *An introduction to structural optimization*. Berlin Heidelberg: Springer Netherlands.
6. Sokolowski, J., Zolesio, J. P. (2003). *Introduction to shape optimization*. Philadelphia, PA: Society for Industrial and Applied Mathematics (SIAM).
7. Wall, W. A., Frenzel, M. A., Cyron, C. (2008). Isogeometric structural shape optimization. *Computer Methods in Applied Mechanics & Engineering*, 197(33–40), 2976–2988. DOI 10.1016/j.cma.2008.01.025.
8. Gallagher, R. H., Zienkiewicz, O. C. (1973). Optimum structural design: theory and applications. *Proceedings of the IEEE*, 66(3), 360–361.
9. Braibant, V., Fleury, C. (1984). Shape optimal design using B-splines. *Computer Methods in Applied Mechanics & Engineering*, 44(3), 247–267. DOI 10.1016/0045-7825(84)90132-4.
10. Qian, X. P. (2010). Full analytical sensitivities in NURBS based isogeometric shape optimization. *Computer Methods in Applied Mechanics and Engineering*, 199(29–32), 2059–2071. DOI 10.1016/j.cma.2010.03.005.
11. Xu, G., Kwok, T. H., Wang, C. C. L. (2017). Isogeometric computation reuse method for complex objects with topology-consistent volumetric parameterization. *Computer-Aided Design*, 91, 1–13. DOI 10.1016/j.cad.2017.04.002.
12. Qian, X., Sigmund, O. (2011). Isogeometric shape optimization of photonic crystals via Coons patches. *Computer Methods in Applied Mechanics and Engineering*, 200(25–28), 2237–2255. DOI 10.1016/j.cma.2011.03.007.
13. Kostas, K. V., Ginnis, A. I., Politis, C. G., Kaklis, P. D. (2017). Shape-optimization of 2D hydrofoils using an isogeometric BEM solver. *Computer-Aided Design*, 82(13), 79–87. DOI 10.1016/j.cad.2016.07.002.
14. Hughes, T. J. R., Cottrell, J. A., Bazilevs, Y. (2005). Isogeometric analysis: CAD, finite elements, NURBS, exact geometry and mesh refinement. *Computer Methods in Applied Mechanics and Engineering*, 194(39–41), 4135–4195. DOI 10.1016/j.cma.2004.10.008.
15. Xu, G., Kwok, T. H., Wang, C. C. L. (2017). Isogeometric computation reuse method for complex objects with topology-consistent volumetric parameterization. *Computer-Aided Design*, 91, 1–13. DOI 10.1016/j.cad.2017.04.002.
16. Charawi, L. A. (2017). Isogeometric overlapping Schwarz preconditioners for the Bidomain reaction-diffusion system. *Computer Methods in Applied Mechanics & Engineering*, 319, 472–490. DOI 10.1016/j.cma.2017.03.012.
17. Gu, J. L., Zhang, J. M., Li, G. Y. (2012). Isogeometric analysis in BIE for 3-D potential problem. *Engineering Analysis with Boundary Elements*, 36(5), 858–865. DOI 10.1016/j.enganabound.2011.09.018.
18. Coox, L., Atak, O., Vandepitte, D., Desmet, W. (2017). An isogeometric indirect boundary element method for solving acoustic problems in open-boundary domains. *Computer Methods in Applied Mechanics & Engineering*, 316(5), 186–208. DOI 10.1016/j.cma.2016.05.039.
19. Michael, R. D., Bert, J., Bernd, S. (2008). Adaptive isogeometric analysis by local h-refinement with T-splines. *Computer Methods in Applied Mechanics and Engineering*, 199(5–8), 264–275.
20. Bazilevs, Y., Calo, V. M., Cottrell, J. A., Evans, J. V., Hughes, T. J. R. et al. (2010). Isogeometric analysis using T-splines. *Computer Methods in Applied Mechanics and Engineering*, 199(5–8), 229–263. DOI 10.1016/j.cma.2009.02.036.

21. Lu, J. (2011). Isogeometric contact analysis: geometric basis and formulation for frictionless contact. *Computer Methods in Applied Mechanics and Engineering*, 200(5–8), 726–741. DOI 10.1016/j.cma.2010.10.001.
22. Lorenzis, L. D., Wriggers, P., Hughes, T. J. R. (2014). Isogeometric contact: a review. *GAMM-Mitteilungen*, 37(1), 85–123. DOI 10.1002/gamm.201410005.
23. Li, K., Qian, X. (2011). Isogeometric analysis and shape optimization via boundary integral. *Computer-Aided Design*, 43(11), 1427–1437. DOI 10.1016/j.cad.2011.08.031.
24. Qian, X., Sigmund, O. (2011). Isogeometric shape optimization of photonic crystals via Coons patches. *Computer Methods in Applied Mechanics and Engineering*, 200(25–28), 2237–2255. DOI 10.1016/j.cma.2011.03.007.
25. Fusseder, D., Simeon, B., Vuong, A. V. (2015). Fundamental aspects of shape optimization in the context of isogeometric analysis. *Computer Methods in Applied Mechanics and Engineering*, 286(1), 313–331. DOI 10.1016/j.cma.2014.12.028.
26. Wang, Z. P., Turteltaub, S. (2015). Isogeometric shape optimization for quasi-static processes. *International Journal for Numerical Methods in Engineering*, 104(5), 347–371. DOI 10.1002/nme.4940.
27. Kostas, K. V., Ginnis, A. I., Politis, C. G. (2017). Shape-optimization of 2D hydrofoils using an isogeometric BEM solver. *Computer-Aided Design*, 82(13), 79–87. DOI 10.1016/j.cad.2016.07.002.
28. Lieu, Q. X., Lee, J. (2017). Multi-resolution topology optimization using isogeometric analysis. *International Journal for Numerical Methods in Engineering*, 323(256), 272–302.
29. Qian, X. (2013). Topology optimization in B-spline space. *Computer Methods in Applied Mechanics and Engineering*, 256(3), 15–35. DOI 10.1016/j.cma.2013.06.001.
30. Tavakoli, R., Mohseni, S. M. (2014). Alternating active-phase algorithm for multimaterial topology optimization problems: a 115-line MATLAB implementation. *Structural and Multidisciplinary Optimization*, 49(4), 621–642. DOI 10.1007/s00158-013-0999-1.
31. Park, J., Sutradhar, A. (2015). A multi-resolution method for 3D multi-material topology optimization. *Computer Methods in Applied Mechanics and Engineering*, 285(1), 571–586. DOI 10.1016/j.cma.2014.10.011.
32. Herrema, A. J., Wiese, N. M., Darling, C. N., Ganapathysubramanian, B., Krishnamurthy, A. et al. (2017). A framework for parametric design optimization using isogeometric analysis. *Computer Methods in Applied Mechanics and Engineering*, 316(3), 944–965. DOI 10.1016/j.cma.2016.10.048.
33. Ding, C. S., Cui, X. Y., Li, G. Y. (2016). Accurate analysis and thickness optimization of tailor rolled blanks based on isogeometric analysis. *Structural and Multidisciplinary Optimization*, 54(4), 871–887. DOI 10.1007/s00158-016-1448-8.
34. Piegl, L. A., Tiller, W. (1995). *The Nurbs book*. Berlin Heidelberg: Springer-Verlag.
35. Ruess, M., Schillinger, D., Özcan, A. I., Rank, E. (2014). Weak coupling for isogeometric analysis of non-matching and trimmed multi-patch geometries. *Computer Methods in Applied Mechanics and Engineering*, 269, 46–71. DOI 10.1016/j.cma.2013.10.009.
36. Zhao, G., Du, X., Wang, W., Liu, B., Fang, H. (2017). Application of isogeometric method to free vibration of Reissner–Mindlin plates with non-conforming multi-patch. *Computer-Aided Design*, 82, 127–139. DOI 10.1016/j.cad.2016.04.006.
37. Brockman, R. A. (1987). Geometric sensitivity analysis with isoparametric finite elements. *Communications in Applied Numerical Methods*, 3(6), 495–499. DOI 10.1002/cnm.1630030609.
38. Nitsche, J. (2013). Über ein variationsprinzip zur losung von dirichlet-problemen bei verwendung von teilräumen, die keinen randbedingungen unterworfen sind. *Abhandlungen aus dem Mathematischen Seminar der Universität Hamburg*, 36, 9–15. DOI 10.1007/BF02995904.
39. Klarbring, A. (2008). *An introduction to structural optimization*. Berlin Heidelberg: Springer Netherlands.
40. Braibant, V., Fleury, C. (1984). Shape optimal design using B-splines. *Computer Methods in Applied Mechanics and Engineering*, 44(3), 247–267. DOI 10.1016/0045-7825(84)90132-4.
41. Bletzinger, K. U., Firl, M., Linhard, J., Wüchner, R. (2010). Optimal shapes of mechanically motivated surfaces. *Computer Methods in Applied Mechanics and Engineering*, 199(5–8), 324–333. DOI 10.1016/j.cma.2008.09.009.

42. Nagy, A. P., Abdalla, M. M., Zafer, G. (2010). Isogeometric sizing and shape optimisation of beam structures. *Computer Methods in Applied Mechanics & Engineering*, 199(17–20), 1216–1230. DOI 10.1016/j.cma.2009.12.010.
43. Liu, H. L., Yang, D. X., Wang, X., Wang, Y. T., Liu, C. et al. (2018). Smooth size design for the natural frequencies of curved Timoshenko beams using isogeometric analysis. *Structural and Multidisciplinary Optimization*, 59(4), 1143–1162. DOI 10.1007/s00158-018-2119-8.
44. Wang, Z. P., Hien, P. L. (2018). Optimal form and size characterization of planar isotropic petal-shaped auxetics with tunable effective properties using IGA. *Composite Structures*, 201(10), 486–502. DOI 10.1016/j.compstruct.2018.06.042.
45. Wang, Y. Z., Liao, Z. Y., Shi, S. Y., Wang, Z. P., Hien, P. L. (2020). Data-driven structural design optimization for petal-shaped auxetics using isogeometric analysis. *Computer Modeling in Engineering & Sciences*, 122(2), 433–458. DOI 10.32604/cmcs.2020.08680.
46. Wang, Y. Z., Wang, Z. P., Xia, Z. H., Hien, P. L. (2018). Structural design optimization using isogeometric analysis: a comprehensive review. *Computer Modeling in Engineering & Sciences*, 117(3), 455–507. DOI 10.31614/cmcs.2018.04603.